

# Differential Charge Sensing and Charge Delocalization in a Tunable Double Quantum Dot

L. DiCarlo, H. J. Lynch, A. C. Johnson, L. I. Childress, K. Crockett, C. M. Marcus  
*Department of Physics, Harvard University, Cambridge, Massachusetts 02138*

M. P. Hanson, A. C. Gossard  
*Materials Department, University of California, Santa Barbara, California 93106*

We report measurements of a tunable double quantum dot, operating in the quantum regime, with integrated local charge sensors. The spatial resolution of the sensors is sufficient to allow the charge distribution within the double dot system to be resolved at fixed total charge. We use this readout scheme to investigate charge delocalization as a function of temperature and strength of tunnel coupling, showing that local charge sensing allows an accurate determination of interdot tunnel coupling in the absence of transport.

Coupled semiconductor quantum dots have proved a fertile ground for exploring quantum states of electronic charge and spin. These “artificial molecules” are a scalable technology with possible applications in information processing. New kinds of classical computation may arise from quantum dots configured as single electron switches [1] or as building blocks for cellular automata [2]. Ultimately, coupled quantum dots may provide a quantum computing platform where the charge states and/or spins of electrons play a vital role [3]. Charge-state superpositions may be probed using tunnel-coupled quantum dots, which provide a tunable two-level system whose two key parameters, the bare detuning  $\epsilon$  and tunnel coupling  $t$  between two electronic charge states [4], can be controlled electrically.

In this Letter, we investigate experimentally a quantum two-level system, realized as left/right charge states in a gate-defined GaAs double quantum dot, using local electrostatic sensing (see Fig. 1). In the absence of tunneling, the states of the two-level system are denoted  $(M+1, N)$  and  $(M, N+1)$ , where the pair of integers refer to the number of electrons on the left and right dots. For these two states, the total electron number is fixed, with a single excess charge moving from one dot to the other as a function of gate voltages. When the dots are tunnel coupled, the excess charge becomes delocalized and the right/left states hybridize into symmetric and antisymmetric states.

Local charge sensing is accomplished using integrated quantum point contacts (QPC’s) positioned at opposite sides of the double dot. We present a model for charge sensing in a tunnel-coupled two-level system, and find excellent agreement with experiment. The model allows the sensing signals to be calibrated using temperature dependence and measurements of various capacitances. For significant tunnel coupling,  $0.1k_B T_e \lesssim t < \Delta$  ( $T_e$  is electron temperature,  $\Delta$  is the single-particle level spacing of the individual dots), the tunneling rate  $t$  (in units of energy) can be extracted quantitatively from the charge sensing signal, providing an improved method for mea-

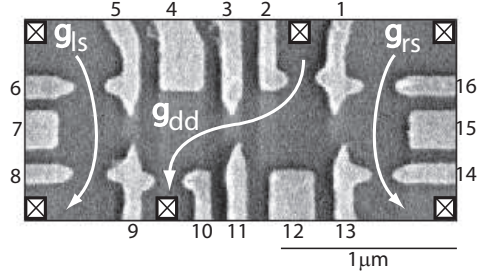


FIG. 1: SEM micrograph of a device similar to the measured device, consisting of a double quantum dot with quantum point contact charge sensors formed by gates 8/9 (13/14) adjacent to the left (right) dot. Series conductance  $g_{dd}$  through the double dot was measured simultaneously with conductances  $g_{ls}$  and  $g_{rs}$  through the left and right sensors.

suring tunneling in quantum dot two-level systems compared to transport methods [4].

Charge sensing using a QPC was first demonstrated in Ref. [5], and has been used previously to investigate charge delocalization in a single dot strongly coupled to a lead in the classical regime [6], and as a means of placing bounds on decoherence in an isolated double quantum dot [2]. The back-action of a QPC sensor, leading to phase decoherence, has been investigated experimentally [7] and theoretically [8]. Charge sensing with sufficient spatial resolution to detect charge distributions within a double dot has been demonstrated in a metallic system [12, 13]. However, in metallic systems the interdot tunnel coupling cannot be tuned, making the crossover to charge delocalization difficult to investigate. Recently, high-bandwidth charge sensing using a metallic single-electron transistor [9], allowing individual charging events to be counted, has been demonstrated [10]. Recent measurements of gate-defined few-electron GaAs double dots [11] have demonstrated dual-QPC charge sensing down to  $N, M = 0, 1, 2, \dots$ , but did not focus on sensing at fixed electron number, or on charge delocalization. The present experiment uses larger dots, containing  $\sim 200$  electrons each (though still with temperature less than

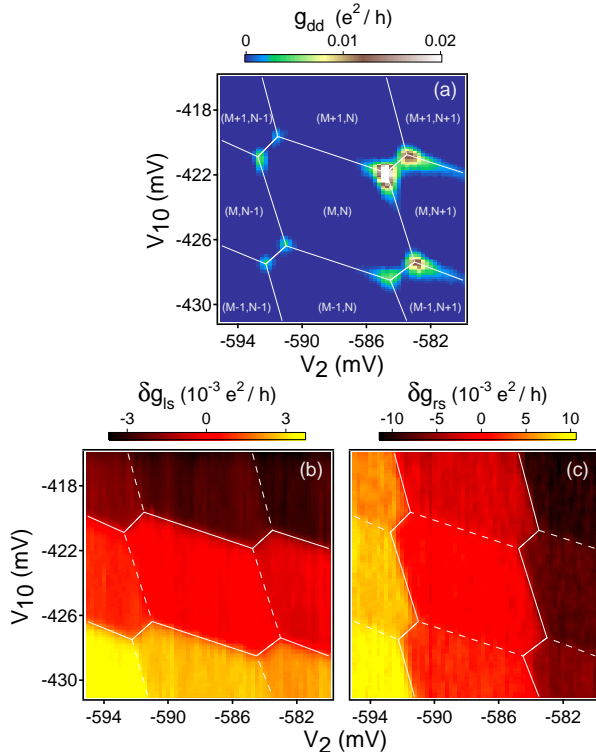


FIG. 2: (a) Conductance through the double dot,  $g_{dd}$ , as a function of gate voltages  $V_2$  and  $V_{10}$ . White lines indicate honeycomb pattern. Within each cell of the honeycomb, electron number on each of the two dots is well defined, with  $M(N)$  referring to electron number in the left (right) dot. (b, c) Simultaneously measured sensing signals from the left (b) and right (c) QPCs,  $\delta g_{ls}$  ( $\delta g_{rs}$ ) are QPC conductances after subtracting a best-fit plane to the center honeycomb to remove the slowly varying direct influence of gates 2 and 10 on QPC conductances. The horizontal pattern in (b) and vertical pattern in (c) demonstrate that each sensor is predominantly sensitive to the charge on the dot it borders, and not the charge of the other dot.

level spacing, see below).

The device we investigate, a double quantum dots with adjacent charge sensors, is formed by sixteen electrostatic gates on the surface of a GaAs/Al<sub>0.3</sub>Ga<sub>0.7</sub>As heterostructure grown by molecular beam epitaxy (see Fig. 1). The two-dimensional electron gas layer, 100 nm below the surface, has an electron density of  $2 \times 10^{11} \text{ cm}^{-2}$  and mobility  $2 \times 10^5 \text{ cm}^2/\text{Vs}$ . Gates 3/11 control the interdot tunnel coupling while gates 1/2 and 9/10 control coupling to electron reservoirs. In this measurement, the left and right sensors were QPCs defined by gates 8/9 and 13/14, respectively; gates 6, 7, 15, and 16 were not energized. Gaps between gates 5/9 and 1/13 were fully depleted, allowing only capacitive coupling between the double dot and the sensors.

Series conductance,  $g_{dd}$ , through the double dot was measured using standard lock-in techniques with a voltage bias of  $5 \mu\text{V}$  at 87 Hz. Simultaneously, conductances

through the left and right QPC sensors,  $g_{ls}$  and  $g_{rs}$ , were measured in a current bias configuration using separate lock-in amplifiers with  $0.5 \text{ nA}$  excitation at 137 and 187 Hz. Throughout the experiment, QPC sensor conductances were set to values in the  $0.1$  to  $0.4 \text{ } e^2/h$  range by adjusting the voltage on gates 8 and 14.

The device was cooled in a dilution refrigerator with base temperature  $T \sim 30 \text{ mK}$ . Electron temperature  $T_e$  at base was  $\sim 100 \text{ mK}$ , measured using Coulomb blockade peak widths with a single dot formed. Single-particle level spacing  $\Delta \sim 80 \mu\text{eV}$  for the individual dots was also measured in a single-dot configuration using nonlinear  $dI/dV$  measurements at finite bias. Single-dot charging energies,  $E_C = e^2/C_o \sim 500 \mu\text{eV}$  for both dots (giving dot capacitances  $C_o \sim 320 \text{ aF}$ ), were extracted from the height (in source-drain voltage) of Coulomb blockade diamonds [14].

Figure 2(a) shows double-dot conductance,  $g_{dd}$ , as a function of gate voltages  $V_2$  and  $V_{10}$ , exhibiting the familiar ‘honeycomb’ pattern of series conductance through tunnel-coupled quantum dots [15, 16, 17]. Peaks in conductance at the honeycomb vertices, the so-called triple points, result from simultaneous alignment of energy levels in the two dots with the chemical potential of the leads. Although conductance can be finite along the honeycomb edges as a result of cotunneling, here it is suppressed by keeping the dots weakly coupled to the leads. Inside a honeycomb, electron number in each dot is well defined as a result of Coulomb blockade. Increasing  $V_{10}$  ( $V_2$ ) at fixed  $V_2$  ( $V_{10}$ ) increases the electron number in the left (right) dot one by one.

Figures 2(b) and 2(c) show left and right QPC sensor signals measured simultaneously with the double-dot conductance,  $g_{dd}$ , shown in Fig. 2(a). The sensor data plotted are  $\delta g_{ls(rs)}$ , the left (right) QPC conductances after subtracting a best-fit plane (fit to the central hexagon) to remove the background slope due to cross-coupling of the plunger gates (gates 2 and 10) to the QPCs. The left sensor shows conductance steps of size  $\sim 3 \times 10^{-3} \text{ } e^2/h$  along the (more horizontal) honeycomb edges where the electron number on the left dot changes by one (solid lines in Fig. 2(b)); the right sensor shows conductance steps of size  $\sim 1 \times 10^{-2} \text{ } e^2/h$  along the (more vertical) honeycomb edges where the electron number of the right dot changes by one (solid lines in Fig. 2(c)). Both detectors show a conductance step, one upward and the other downward, along the  $\sim 45$ -degree diagonal segments connecting nearest triple points. It is along this shorter segment that the total electron number is fixed; crossing the line marks the transition from  $(M + 1, N)$  to  $(M, N + 1)$ . Overall, we see that the transfer of one electron between one dot and the leads is detected principally by the sensor nearest to that dot, while the transfer of one electron between the dots is detected by both sensors, as an upward step in one and a downward step in the other, as expected.

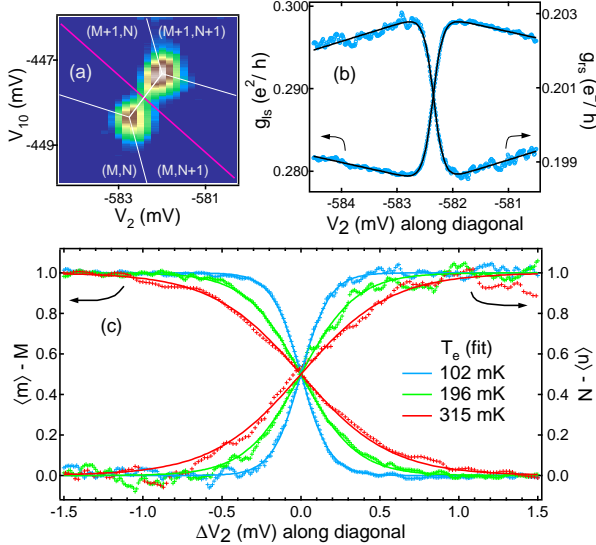


FIG. 3: (a) Double dot conductance  $g_{dd}$  as a function of gate voltages  $V_2$  and  $V_{10}$  in the vicinity of a triple point. Color scale is the same as in Fig. 1(a). The detuning diagonal (red line) indicates the fixed-charge transition between  $(M+1, N)$  and  $(M, N+1)$  swept by gate voltages  $V_2$  and  $V_{10}$ . (b) Left and right QPC conductance with no background subtraction (blue points), along the detuning diagonal, along with fits of the two-level model, Eq. (1) (black curves). See text for fit details. (c) Average excess charge on the left and right dot, at fridge temperatures  $T = 30$  mK (blue), 200 mK (green) and 315 mK (red). Corresponding electron temperature extracted from the fits (solid curves) are 102, 196 and 315 mK using the 315 mK data to calibrate the lever arm (i.e., assuming  $T = T_e$ ) providing the conversion between gate voltage along the diagonal to detuning  $\epsilon$ .

Focusing on interdot transitions at fixed total charge, i.e., transitions from  $(M+1, N)$  to  $(M, N+1)$ , we present charge-sensing data taken along the “detuning” diagonal by controlling gates  $V_2$  and  $V_{10}$ , shown as a red diagonal line between the triple points in Fig. 3(a). Raw data (no background subtracted) for the two QPC charge sensors are shown in Fig. 3(b). The transfer of the excess charge from left dot to right dot causes a step in the conductance of both QPCs, clearly discernable from the background slope resulting from the coupling of gates 2 and 10 to the QPC.

Also shown in Fig. 3(b) are fits to the raw sensor data based on a simple model of local sensing of an isolated two-level system:

$$g_{ls(rs)} = g_{ol(or)} \pm \delta g_{l(r)} \frac{\epsilon}{\sqrt{\epsilon^2 + 4t^2}} \tanh \left( \frac{\sqrt{\epsilon^2 + 4t^2}}{2k_B T_e} \right) + \frac{\partial g_{l(r)}}{\partial \epsilon} \epsilon. \quad (1)$$

The first term on the right in Eq. (1) is the background conductance of the left (right) QPC sensor; the second term represents changes in QPC sensor conductance, assumed to be proportional to the average excess charge on its neighboring dot; the third term represents direct coupling of gates to the QPC. Average excess charge on

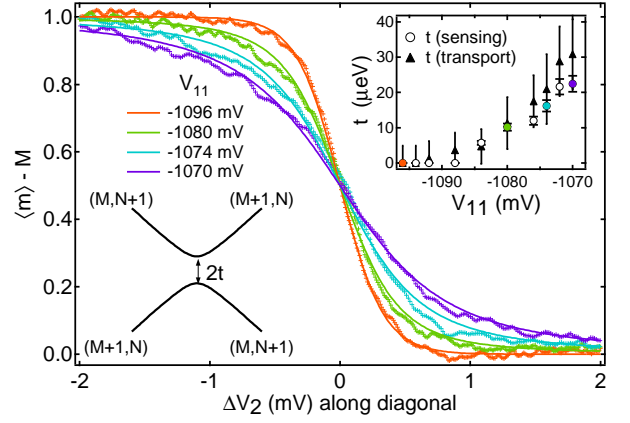


FIG. 4: Left QPC sensor signal along a detuning diagonal (not the same triple point as in Fig. 3) at base temperature, for several interdot tunnel coupling settings controlled by gate voltage  $V_{11}$ . The temperature broadened curve (red) widens as  $V_{11}$  is made less negative, increasing the tunnel coupling,  $t$ . Using  $T_e = 102$  mK in Eq. (2) gives tunnel couplings  $t = 10 \mu\text{eV}$  (green),  $t = 16 \mu\text{eV}$  (turquoise), and  $t = 22 \mu\text{eV}$  (blue). See text for detail of fit. Top right inset: comparison of interdot tunnel coupling  $t$  extracted from sensing (circles) and transport (triangles) measurements, as a function of gate voltage  $V_{11}$ . Colored circles correspond to the transitions shown in the main graph. Lower left inset: Schematic energy diagram of the two-level system model, showing ground and excited states as a function of detuning parameter  $\epsilon$ , with splitting (anticrossing) of  $2t$  at  $\epsilon = 0$ .

each dot depends on the bare detuning  $\epsilon$ , the tunnel coupling  $t$  between the  $(M+1, N)$  and  $(M, N+1)$  states, which determines the quantum mechanical spreading of charge across the two dots, and the electron temperature  $T_e$ , which accounts for effects of thermal excitation into the excited state (within this simple two-level model). As shown in Fig. 2(b), this model gives very good fits to the data. For each trace (left and right sensors), fit parameters are  $g_{ol(or)}$ ,  $\delta g_{l(r)}$ ,  $\frac{\partial g_{l(r)}}{\partial \epsilon}$ , and  $T_e$ . In these data, the tunnel coupling between dots is weak, and we may set  $t = 0$ .

Figure 3(c) shows the effect of increasing electron temperature on the transition width. Here, vertical axes show excess charge (in units of  $e$ ) extracted from fits to QPC sensor conductance data, i.e., the excess charge, ranging from zero to one, is just the second term in Eq. (1) with a scale factor and an offset:

$$\langle m \rangle - M = \frac{1}{2} \left( 1 - \frac{\epsilon}{\sqrt{\epsilon^2 + 4t^2}} \tanh \left( \frac{\sqrt{\epsilon^2 + 4t^2}}{2k_B T_e} \right) \right) \quad (2)$$

$$\langle n \rangle - N = \frac{1}{2} \left( 1 + \frac{\epsilon}{\sqrt{\epsilon^2 + 4t^2}} \tanh \left( \frac{\sqrt{\epsilon^2 + 4t^2}}{2k_B T_e} \right) \right) \quad (3)$$

Data in Fig. 3(c) were taken at refrigerator temperatures of 30 mK (blue), 200 mK (green) and 315 mK (red). Using the 315 mK (red) data to extract a lever arm relating voltage along the diagonal (see Fig. 3(a)) to de-

tuning energy  $\epsilon$ , we find electron temperatures  $T_e = 102(196)$  mK for the blue (green) data.

We next investigate the dependence of the sensing transition on interdot tunneling in the regime of strong tunneling,  $t \gtrsim k_B T_e$ . Figure 4 shows the left QPC sensing signal, again in units of excess charge, along a different detuning diagonal at base temperature for various voltages on the coupling gate 11. For the weakest interdot tunneling shown ( $V_{11} = -1096$  mV), the transition was thermally broadened, i.e., consistent with  $t = 0$  in Eq. (2), and did not become narrower when  $V_{11}$  was made more negative. On the other hand, when  $V_{11}$  was made less negative, the transition widened as the tunneling between dots increased. Taking  $T_e = 102$  mK for all data in Fig. 4 and calibrating voltage along the detuning diagonal by setting  $t = 0$  for the  $V_{11} = -1096$  mV trace allows tunneling rates  $t$  to be extracted from fits of Eq. (2) to the other tunnel-broadened traces. We find  $t = 10 \mu\text{eV}$  (2.4 GHz) (green trace),  $t = 16 \mu\text{eV}$  (3.9 GHz) (turquoise trace), and  $t = 22 \mu\text{eV}$  (5.3 GHz) (blue trace). Again, fits to the simple two-level model are quite good, as seen in Fig. 4.

Finally, we compare interdot tunneling rates,  $t$ , extracted from charge sensing to values found using a transport-based method that takes advantage of the  $t$  dependence of the splitting of resonant-tunneling triple points [4, 18]. In the weak tunneling regime,  $t \ll \Delta$ , the splitting of triple points (honeycomb vertices) along the line separating isochARGE regions  $(M + 1, N)$  and  $(M, N + 1)$  has two components in the plane of gate voltages, denoted for the present device  $\delta V_{10}$  and  $\delta V_2$ . These components can be expressed in terms of various dot capacitances and the tunnel coupling,  $t$ , as

$$\delta V_{10(2)} = \frac{|e|}{C_{g10(g2)}} \left( \frac{C_m}{C_o + C_m} + 2t \frac{C_o - C_m}{e^2} \right). \quad (4)$$

In Eq. (4),  $C_{g10(g2)}$  is the capacitance from gate 10 (2) to the left (right) dot,  $C_o$  is the self-capacitance of each dot, and  $C_m$  is the mutual capacitance between the dots. All these capacitances must be known in order to extract  $t$  from the splitting components  $\delta V_{2(10)}$ . Gate capacitances  $C_{g10(g2)}$  are estimated from honeycomb periods along respective gate voltage axes,  $\Delta V_{2(10)} \sim |e|/C_{g2(g10)} \sim 6.8$  mV. Self-capacitances  $C_o$  can be obtained from double dot transport measurements at finite drain-source bias [4]. However, lacking that data, we instead estimate  $C_o$  from single-dot measurements of Coulomb diamonds [14]. Mutual capacitance  $C_m$  is extracted from the dimensionless splitting  $\delta V_{10(2)}/\Delta V_{10(2)} \sim \frac{C_m}{C_o + C_m} \sim 0.2$ , measured at the lowest tunnel coupling setting.

Interdot tunneling rate  $t$  as a function of voltage on coupling gate 11, extracted both from charge sensing and triple-point separation, are compared in the inset of Fig. 4. The two approaches are in good agreement, with the charge sensing approach giving significantly smaller uncertainty. We note that besides being more sensitive, the charge sensing method for measuring interdot tunneling works when the double dot is fully decoupled from its leads.

In conclusion, we have demonstrated differential charge sensing in a double quantum dot using paired quantum point contact charge sensors. States  $(M + 1, N)$  and  $(M, N + 1)$ , with fixed total charge, are readily resolved by the sensors, and serve as a two-level system with a splitting of left/right states controlled by gate-defined tunneling between states. A model of local charge sensing based on a thermally occupied two-level system with tunneling agrees well with the data. Finally, the width of the  $(M + 1, N) \rightarrow (M, N + 1)$  transition measured with this sensing technique can be used to extract the tunnel coupling with high accuracy.

We thank M. Lukin, B. Halperin and W. van der Wiel for valuable discussions, and N. Craig for experimental assistance. We acknowledge support by the ARO under DAAD19-02-1-0070, DARPA under the QuIST program, the NSF under DMR-0072777 and the Harvard NSEC, Lucent Technologies (HJL), and the Hertz Foundation (LIC).

---

- [1] I.H. Chan *et al.*, Appl. Phys. Lett. **80**, 1818 (2002).
- [2] S. Gardelis *et al.*, Phys. Rev. B **67**, 073302 (2003).
- [3] H.-A. Engel *et al.*, arXiv:cond-mat/0309023 (2003).
- [4] W.G. van der Wiel *et al.*, Rev. Mod. Phys. **75**, 1 (2003).
- [5] M. Field *et al.*, Phys. Rev. Lett. **70**, 1311 (1993).
- [6] D.S. Duncan *et al.*, Appl. Phys. Lett. **74**, 1045 (1999).
- [7] E. Buks *et al.*, Nature **391**, 871 (1998).
- [8] I. L. Aleiner, N. S. Wingreen, Y. Meir, Phys. Rev. Lett. **79**, 3740 (1997); Y. Levinson, Europhys. Lett. **39**, 299 (1997).
- [9] R.J. Schoelkopf *et al.*, Science **280**, 1238 (1998).
- [10] Wei Lu *et al.*, Nature **423**, 422 (2003).
- [11] J.M. Elzerman *et al.*, Phys. Rev. B **67**, R161308 (2003).
- [12] I. Amlani *et al.*, Appl. Phys. Lett. **71**, 1730 (1997).
- [13] T.M. Buehler *et al.*, Appl. Phys. Lett. **82**, 577 (2003).
- [14] L.P. Kouwenhoven *et al.*, in *Mesoscopic Electron Transport*, edited by L.L. Sohn, L.P. Kouwenhoven, and G. Schön (Kluwer, Dordrecht, 1997).
- [15] H. Pothier *et al.*, Europhys. Lett. **17**, 249 (1992).
- [16] R.H. Blick *et al.*, Phys. Rev. B **53**, 7899 (1996).
- [17] C. Livermore *et al.*, Science **274**, 5291 (1996).
- [18] R. Ziegler *et al.*, Phys. Rev. B **62**, 1961 (2000)